A 3D Shape Tracking Algorithm for Flexible Needle in Brain Surgery

PhuBao Nguyen[1,2], Jayoung Kim[2], Eunpyo Choi[1,2], Byungjeon Kang[2*], Jong-Oh Park[1,2*] and Chang-Sei Kim[1,2*]

[1] School of Mechanical Engineering, Chonnam National University, Gwangju, 61186, Korea;

[2] Medical Microrobot Center, Robot Research Initiative, Chonnam National University, Gwangju, 61011, Korea;

*Corresponding author Email: bjkang8204@jnu.ac.kr; jop@jnu.ac.kr; ckim@jnu.ac.kr

Telephone: +82-62-530-5230; fax: +82-62-530-5238

Abstract

This paper poposed an optimal tracking technique in three dimensional space of the needle shape intraoperation. The technique make use of stereo vision and epipolar geometry to reconstruct corresponding point lying on the centerline of the needle captured from two camera. Using epipolar relationship between two sets of corresponding point, the spatial position of the centerline of the needle is reconstructed with respect to world coordinate system. As a result, the spatial position as well as geometric shape of the needle is tracked in near real-time interval.

1 Introduction

In recent years, much attention has been paid for minimally invasive brain surgery with the treatment of controllable flexible needle due to its vast advantages [1, 2]. Especially, it has not only a minimal affected area but also a much shorter period of recovery time compared to conventional open surgery. Most of the recent steerable needle system uses its tip to steer and control the direction as well as its 3D geometric shape [3]. However, due to the limitation in stiffness of existing needle, its tip and shaft may cause the damages for the brain [4]. To control the movement of the needle precisely as well as to avoid the damages of brain, three dimensional needle tracking control is required but implementation is challenging.

Some techniques are available for 3D shape tracking of the needle in surgery such as using sonography machine, MRI imaging device, CT imaging [5-10]. However, due to their limitation in term of poor image quality and long generating time, they are currently not applicable in real-time robot assisted surgery.

Hence, to overcome those challeges arised in needle control for brain surgery, we propose an optimal technique to track both tip point and entire geometric shape of the needle in three dimension space using stereo vision and 3D reconstruction algorithm. The tracking experiment is carried out with a flexible needle fixed inside the workspace of stationary stereo camera where the distance from cameras to the needle is set approximately 250 mm. By the suggested methods, first, the stereo camera is precisely calibrated with a standard checker board of size 11x11 squared grids in each dimension to get projection and each fundamental matrix. Next, stereo image pair of the fixed needle is captured by both cameras sequentially and saved in memory for post-processing. In image processing step, image of the needle is segmented and then complemented to get its entire shape in 2D. To reduce the image size by eliminating unnecessary information, a skeletonization technique is applied for finding the centerline of needle shape in each image. Each single white-pixel belonging to centerline of left and right image is then saved in two point set, respectively. Epipolar geometry and fundamental matrix is utilized to determine corresponding point pair between two point. When having corresponding point pair, 3D reconstruction algorithm is applied to determine position of each single point belonging to centerline of needle shape with critically high accuracy: positional error attains ± 0.25 mm when the distance from camera to the needle is 250mm. Therefore, 3D shape of the needle in space is properly determined by a point set which describes its centerline.

To confirm the accuracy of 3D reconstruction, projection algorithm proposed by R. Harley and A. Zisserman and PI. Corke with camera model is applied [11, 12]. The experimental results show that the mean error of the projection attains 30.3 pixels within approximately one second of processing time. In conversion to real world coordinate, the mean error attain 1.01 mm. We expected that the proposed tracking technique will provide a significant contribution to improve accuracy and processing time of recent needle tracking technique and could be applied in practice.

The paper is organized as follows. In Section 2, the centerline extration technique used in 2D images wil be introduced. The application of epipolar geometry extraction technique in corresponding point check will be shown at Section 3. The algorithms to reconstruct 3D position and geometric shape of the needle in space will be explained in Section 4. And then, the experimental results and conclusion will be provided at the last parts.

2 Centerline extraction

Figure 1 describes the images of the needle captured by the stereo camera. These images are pre-processed to enhance the contrast of the edge and equalize the histogram. Furthermore, all of the noise around the border of the image will be eliminate to get the best segmentation of the needle shape.

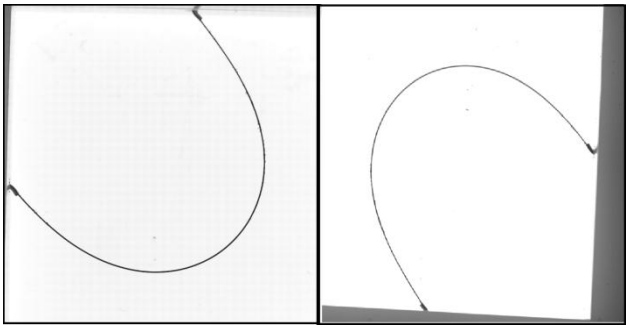

Figure 1 Image of the needle captured by two cameras

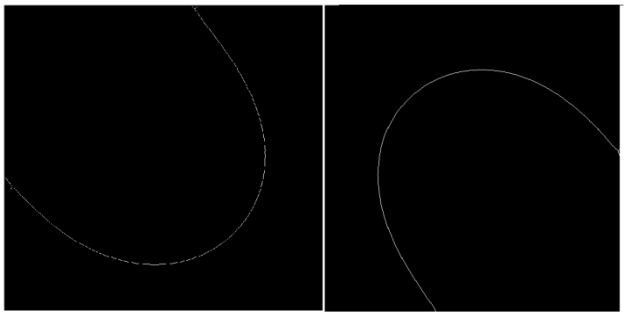

Figure 2 Image of the needle after skeletonization

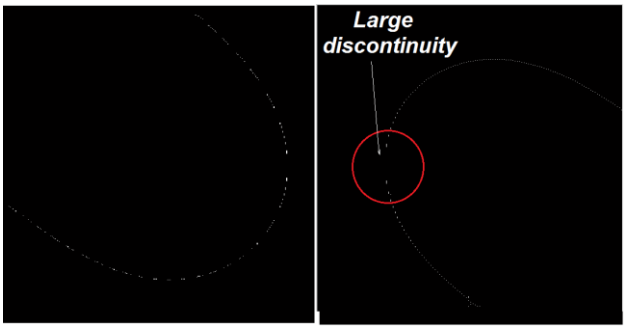

Figure 3 Large discontinuity image of the needle centerline after skeletonization reduced by 5 times

For the preprocesssed image in Figure 1, the centerline extraction is carried out with skeletonization technique implemented in Matlab 2014b as shown in Figure 2. After skeletonization processing for each image, we can obtain a set of centerline point in two-dimensional space as of S_p and S_q in (1).

$$S_p = \begin{bmatrix} x_p(1) & y_p(1) \\ \dots & \dots \\ x_p(i) & y_p(i) \end{bmatrix} \text{ and } S_q = \begin{bmatrix} x_q(1) & y_q(1) \\ \dots & \dots \\ x_q(j) & y_q(j) \end{bmatrix} \quad (1)$$

To save memory as well as to reduce the processing time in the next step, the number of point in each set could be reduced by k times. It is a trade-off between processing time and resolution of accuracy. Therefore, to remain a proper precision in tracking geometric shape of the needle, the condition should be hold as $k \leq 5$ with $k \in N^+$. In this condition, if $k > 5$, there is a large discontinuous distance at the centerline of the needle shape and it may cause the difficulties or mismatch for curve fitting step. Figure 3 shows an example of large discontinutity of this.

3 Corresponding point check

3.1 Epipolar geometry

In order to reconstruct positions of each centerline point of needle shape, we have to determine the corresponding points in stereo image pair. In stereo vision, epipolar geometry describes the relationship between two images p and q captured by two cameras located at spatial points C_p and C_q, respectively. Epipolar geometry is normally used to check the correspondence between two points or two point sets from two calibrated cameras [12].

Assuming that M is a spatial point located at the centerline of the needle shape, M can be captured by stereo camera and appeared in two image as m_p and m_q, respectively (with $m_p \in S_p, m_q \in S_q$). Figure 4 describes epipolar geometry between two corresponding images p and q in relation with the epipolar plane and baseline. The epipolar geometry in this case could be used to determine whether a point m_p belonging to image p is the correspondence of m_q in image q or not.

Furthermore, a fundamental matrix F describes the constraint between two corresponding points m_p and m_q projected from a spatial point M in three dimentional space. The point m_p and m_q from two images is consider as corresponding point if and only if the below constraint is hold:

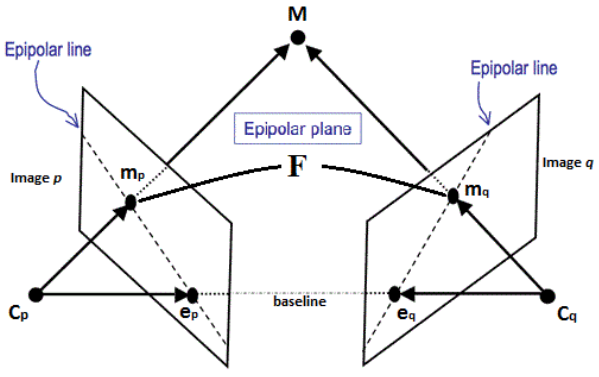

Figure 4 Epipolar geometry between two images

$$m_p{}^T F m_q = 0 \quad (2)$$

where $m_p{}^T F$ is the epipolar line started from epipole e_q on which the point m_q must lies on.

Therefore, in order to check if a point in image p is the correspondence of another point in image q, we only need to check whether the constraint in (2) is zero.

3.2 Fundamental matrix derivation

The fundamental matrix of epipolar geometry can be described and derived in many ways. One of the most well-known technique is introduced by Hartley and Zisserman in [12]. To approach the fundamental matrix method, camera calibration is firstly carried out with a standard checkerboard of size 11x11 squared grids [13], where the size of each square is 2x2 mm. After calibration step, the camera's intrinsic and extrinsic parameters are properly obtained.

Denote that the intrinsic and extrinsic of two camera are K_p and $[R_p|t_p]$ for camera p, K_q and $[R_q|t_q]$ for image q, respectively. Projection matrices of two views p and q, where P_p and P_q are obtained as in the following equation,

$$P_p = K_p[R_p|t_p] \text{ and } P_q = K_q[R_q|t_q] \quad (3)$$

If we assume that the world coordinate system is set coincidently to the camera coordinate system of the view p, then P_p and P_q now become:

$$P_p = K_p[I|0_{3\times1}] \text{ and } P_q = K_q[R|t] \quad (4)$$

where $[R|t]$ is the transformation matrix from the camera coordinate system of the view p to that of view q.

Then, the fundamental matrix corresponding to two views of the stereo camera can be described as in (5).

$$F = [P_q C]_\times P_p P^+ = K_q{}^{-T} R K_p{}^T [K_p R^T t]_\times = K_q{}^{-T} R [R^T t]_\times K_p{}^{-1} = K_q{}^{-T} R K_p{}^T [e_p]_\times \quad (5)$$

where $P_p{}^+ = [K_p{}^{-1} \quad 0_{3\times1}^T]^T$ is the pesudo-inverse of P_p, $C = [0_{3\times1} \quad 1]^T$ is camera center position and the epipoles of two corresponding images can be obtained as in (6)

$$e_p = P_p \begin{bmatrix} -R^T t \\ 1 \end{bmatrix} \text{ and } e_q = P_q \begin{bmatrix} 0_{3\times1} \\ 1 \end{bmatrix} = K_q t \quad (6)$$

where the right subscript "×" indicates a skew-symmetric matrix.

3.3 Corresponding point selection

As described in Section 3.1, two points that is corresponding point pair m_p and m_q are obtained when $m_p{}^T F m_q = 0$ is satisfied. In order to check this constraint between two point set S_p and S_q in Section 2, a pencil epipolar line $l_q = m_p{}^T F$ in epipolar plane is drawn, which starts from two point m_p and e_p of image p, go through epipole e_q of the image q. The line l_q is formed by (7).

$$l_q = m_p{}^T F = [a \quad b \quad c \quad 1]^T \quad (7)$$

in which, the coefficients a, b, c satisfies line equation in 2D plane $ax + by + c = 0$.

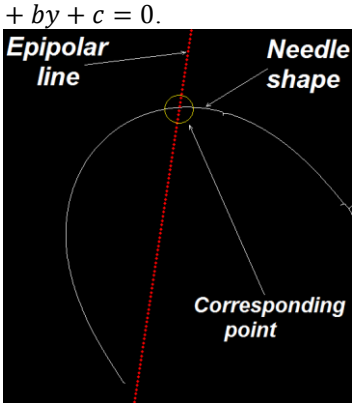

Figure 5 Epipolar line l_q and its intersection with needle shape

Therefore, the corresponding point of m_p in image q is the intersection between epipolar line l_q and the needle shape as illustrated in Figure 5.

However, due to the error in calibration process, the constraint $m_p{}^T F m_q$ is not completely equal to zero. Practically, we utilize this constraint as

$$m_p{}^T F m_q \leq 10^{-4} \quad (8)$$

As our experimental results showed that the reconstruction error of a single point became less than 0.3 mm within this constraint.

3.4 Distance map

It is easy to check the corresponding point pair between two point set S_p and S_q by iterating $i \times j$ times steps in Section 3.3. However it is not a smart way to do because of memory burden and computation time consumption. Instead, we propose the use of distance map with only one matrix computation. It is named distance map since the constraint $m_p{}^T F m_q$ describes the distance from point m_q to epipolar line $l_q = m_p{}^T F$.

Distance map is constructed by:

$$D_{i\times j} = [S_p{}^T]_{i\times3}[F]_{3\times3}[S_q]_{3\times j} \quad (9)$$

in which row-i of D describes the distance from the point $S_p(i)$ to the epipolar line $l_{qi} = m_{pi}{}^T F$.

Figure 6 illustrates a typical distance map by using fundamental matrix F and epipolar geometry. The dark color shows low value of distance, and inversely, the light color means high value of distance.

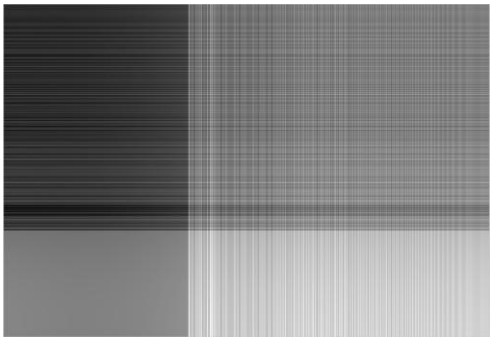

Figure 6 Distance map created by epipolar geometry

Practically, we will search for all position in distance map D which has value $D_{i\times j} < 10^{-4}$. The set of corresponding point pair will be determined by:

$$S = [S_p(i)\ \ S_q(j)] \tag{10}$$

where $D(i,j) \leq 10^{-4}$. By reconstructing the distance map, imaging processing time for checking corresponding point is greatly reduced from approximately 19 second down to 1.01 second.

4 3D reconstruction of the needle shape

Refer to our previous research results [14], we have proposed a numerical formula to reconstruct a 3D point from two corresponding points of stereo images. Although the thereoritical formula comes from X-ray image, we proved that our method can be applied to digital image as well.

In brief, assumed that two points $m_p = [x_p\ y_p]^T$ and $m_q = [x_q\ y_q]^T$ are corresponding points, obtained from projection of a 3D point $M = [X\ \ Y\ \ Z\ \ 1]^T$ onto two images p and q, respectively. Subsequently, the position of M is obtained by solving the following equation:

$$M = H^{-1} \cdot M' \tag{11}$$

$$\lambda_p = \frac{x_q.B_{2,4} - y_q.B_{1,4}}{(B_{1,1}.x_p + B_{1,2}.y_p + B_{1,3}).y_q - x_q.(B_{2,1}.x_p + B_{2,2}.y_p + B_{2,3})} \tag{12}$$

where, $M' = \lambda_p.[m_p^T\ \ 1/\lambda_p]^T$ is reconstructed 3D point in camera coordinate, $B_{3\times4} = K_q.H^{-1}$ is a transition matrix, H is a 4×4 infinity homography matrix [12] and K_q is intrinsic matrix of image q obtained from calibration step. Replace all of these parameters into Equation (12), we obtain the 3D position of point M reconstructed from stereo images p and q.

Repeat the same procedure to the corresponding point set S determined in Section 3.4, the position and geometric shape of the needle is reconstructed in three dimensional space.

5 Experimental Results

In this experiment, a three dimensional needle shape is fixed inside the region of interest of calibrated stereo camera as illustrated in Figure 7 and 8. The shape of the needle can be controlled by a knob in manually.

First, the stereo camera is calibrated with standard checkerboard to get intrinsic and extrinsic parameter for 3D reconstruction. And then, it captures the corresponding images of the needle and carries out the 3D construction to get 3D position and geometric shape of the needle. Finally, the position and geometric shape of the needle is reconstructed by using algorithm proposed in Section 4. The results are illustrated shown at Figure 9 and Figure 10.

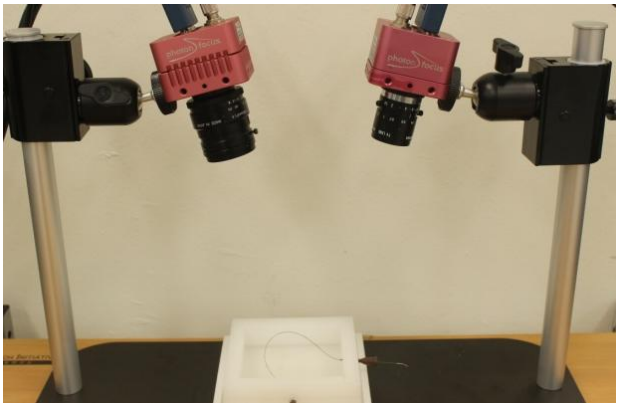

Figure 7 Setup of the experiment

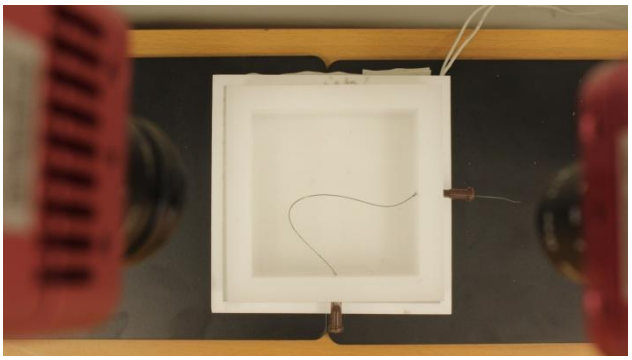

Figure 8 Needle shape is fixed inside workspace of stereo camera

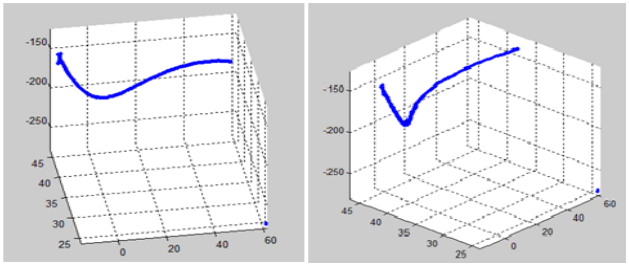

Figure 9 Different view of reconstructed needle shape with full point connected

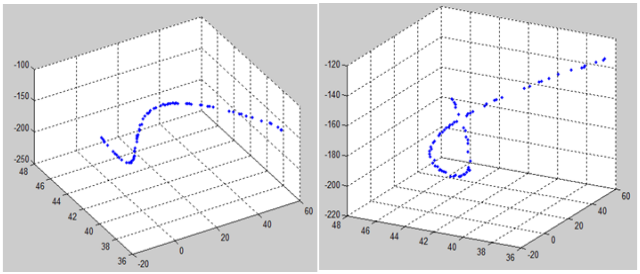

Figure 10 Different view of reconstructed needle shape with the number of points is reduced by 4 times

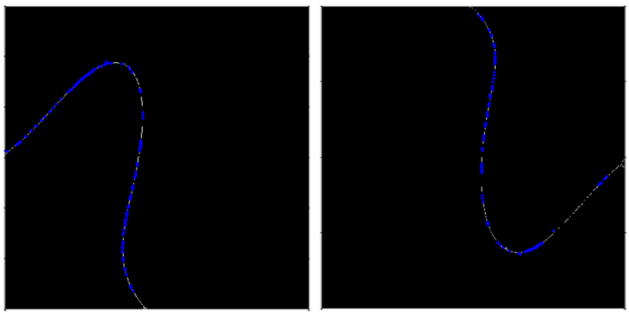

Figure 11 Projection of 3D point set back into left and right stereo images

After 3D reconstruction, to confirm the accuracy of the suggested method, we used camera model proposed in *The Machine Vision Toolbox* by PI Corke to project 3D point set back into original images. The result of projection is shown in Figure 11.

In this case, we used Mean Error to estimate the error in projection step.

$$ME = \frac{d}{n} \tag{13}$$

where d is the minimum distance from a single projected point (blue dot) to the 2D needle centerline (white line) and n is the number of reconstructed point.

The mean error shows that the projection error attains 30.3 pixel in image coordinate. After that, we convert the error from image coordinate to real world coordinate by multiplying the error in pixel with pixel size provided in datasheet of the camera. The result indicates that the error is 1.01 mm.

Furthermore, we calculate processing time to reconstruct the needle shape in five cases, in which the number of reconstructed point is reduced by *k*-times. The result is shown in Table 1 where our suggested method with distance matrix algorithm will significantly reduce the computation time.

Table 1 Processing time to reconstruct needle shape with/without distance matrix

k-number	Number of point	Processing time (without distance matrix)	Processing time (with distance matrix)
1	331	19.21 s	1.01 s
2	165	11.56 s	0.59 s
3	110	8.54 s	0.43 s
4	83	6.89 s	0.48 s
5	65	5.13 s	0.29 s

6 Conclusion

In this paper, we proposed an optimal tracking technique of flexible needle for brain surgery. This technique can track both position and geometry shape of the needle in real-time with high accuracy. The mean error attains 30.1 pixel in image coordinate and 1.01 mm when converted into real world coordinate. The epipolar constraint ${m_p}^T F m_q \leq 10^{-4}$ contribute mostly to the accuracy improvements of the suggested method. Furthermore, by utilizing distance matrix, the processing time is significantly reduced, approximately 20 times faster than the technique using $i \times j$ times iteration for checking proper constraint. This technique remains a weakness especially when dealing with noisy data. This is also our work in the future to improve so that it could be applied in real medical application.

7 Acknowledgement

This research was supported by the Next-generation Medical Device Development Program for Newly-Created Market of the National Research Foundation (NRF) funded by the Korean government, MSIP(No.2015M3D5A1065682).

8 Literatures

[1] J. I. Lee, "The current status of deep brain stimulation for the treatment of Parkinson disease in the Republic of Korea," Journal of movement disorders, Vol. 8, No. 3, 2015, pp. 115.

[2] J. Engh, G. Podnar, S. Khoo, and C. Riviere, "Flexible needle steering system for percutaneous access to deep zones of the brain," in Bioengineering Conference, 2006. Proceedings of the IEEE 32nd Annual Northeast, 2006, pp. 103-104.

[3] D. Glozman and M. Shoham, "Image-guided robotic flexible needle steering," IEEE Transactions on Robotics, Vol. 23, No. 3, 2007, pp. 459-467.

[4] M. D. O'Leary, C. Simone, T. Washio, K. Yoshinaka, and A. M. Okamura, "Robotic needle insertion: Effects of friction and needle geometry," in Robotics and Automation, 2003. Proceedings on ICRA'03 IEEE International Conference, Vol. 2, 2003, pp. 1774-1780.

[5] M. Abayazid, P. Moreira, N. Shahriari, S. Patil, R. Alterovitz, and S. Misra, "Ultrasound-guided three-dimensional needle steering in biological tissue with curved surfaces," Medical engineering & physics, Vol. 37, No. 1, 2015, pp. 145-150.

[6] M. Abayazid, G. J. Vrooijink, S. Patil, R. Alterovitz, and S. Misra, "Experimental evaluation of ultrasound-guided 3D needle steering in biological tissue," International

journal of computer assisted radiology and surgery, Vol. 9, No. 6, 2014, pp. 931-939.

[7] T. K. Adebar, A. E. Fletcher, and A. M. Okamura, "3-D ultrasound-guided robotic needle steering in biological tissue," IEEE Transactions on Biomedical Engineering, Vol. 61, No. 12, 2014, pp. 2899-2910.

[8] M. Khadem, C. Rossa, N. Usmani, R. S. Sloboda, and M. Tavakoli, "Semi-automated needle steering in biological tissue using an ultrasound-based deflection predictor," Annals of biomedical engineering, Vol. 45, No. 4, 2017, pp. 924-938.

[9] P. Moreira, S. Patil, R. Alterovitz, and S. Misra, "Needle steering in biological tissue using ultrasound-based online curvature estimation," in Robotics and Automation (ICRA), 2014 IEEE International Conference, 2014, pp. 4368-4373.

[10] Y. L. Park, S. Elayaperumal, B. Daniel, S. C. Ryu, M. Shin, J. Savall, et al., "Real-time estimation of 3-D needle shape and deflection for MRI-guided interventions," IEEE/ASME Transactions On Mechatronics, Vol. 15, No. 6, 2010, pp. 906-915.

[11] P. I. Corke, "The Machine Vision Toolbox: a MATLAB toolbox for vision and vision-based control," IEEE robotics & automation magazine, Vol. 12, No. 4, 2005, pp. 16-25.

[12] R. Hartley and A. Zisserman, Multiple view geometry in computer vision: Cambridge university press, 2003.

[13] J. Y. Bouguet, "Camera calibration toolbox for matlab," 2004.

[14] P. B. Nguyen, J.-O. Park, S. Park, and S. Y. Ko, "Medical micro-robot navigation using image processing-blood vessel extraction and X-ray calibration," in 6th IEEE International Conference on Biomedical Robotics and Biomechatronics (BioRob), 2016, pp. 365-370.

7月7日（星期五）Friday，July 7, 2017，Room: M3-04

主题/Topic		设计方法学 Design Methodology
会议室/Room 1		M3-04
Time	Number	Paper Title
09:30-09:50	No.83	一种用于电缆驱动并联机器人系统的精确电缆长度控制的新型绞盘系统 A Novel Winch System for a Precise Cable Length Control of a Cable-driven Parallel Robot System
		XueJun Jin
		School of Mechanical Engineering, Chonnam National University, Gwangju, Korea Medical Microrobot Center, Robot Research Initiative, Chonnam National University, Gwangju, Korea
09:50-10:10	No.21	基于.net Framework C#的控制软件编程平台的设计 The design of automation software development platform based-on .net Framework C#
		马立新，王伟　Jack Ma, Harris Wang
		Automation Platform, CODESYS (China), China
10:10-10:30	No.86	A 3D Shape Tracking Algorithm for Flexible Needle in Brain Surgery
		PhuBao Nguyen
		School of Mechanical Engineering, Chonnam National University, Gwangju, Korea Medical Microrobot Center, Robot Research Initiative, Chonnam National University, Gwangju, Korea
10:30-10:40	海报 Poster session & Tea break	
10:40-11:20	Keynote Speech	从全球商业趋势到机器人市场，产品和核心技术 From Global Business Trends to Robotics Markets, Products and Core Technology
		Prof. Andrew A. Goldenberg
		Chief Technology Officer SkyNet Group Limited, Hong Kong President & Founder of ESI, Canada Professor Emeritus, University of Toronto, Canada
11:20-12:00	Keynote Speech	人工智能与机器人：过去、现在与未来 AI and AI robot: Past, Now and Future
		Prof. Il Hong Suh
		Professor of Hanyang University General Chair of IROS 2016, Korea
12:00-12:50	午餐 Lunch Break	

Asia

ISR

powered by IFR

International Symposium on Robotics

Organizers:

IFR International Federation of Robotics

CRIA China Robot Industry Alliance 中国机器人产业联盟 China Robot Industry Alliance

Shanghai·China

July 6-7,2017